Electrostatic Grafting of Diamond Nanoparticles: A Versatile Route to Nanocrystalline Diamond Thin Films

Hugues A. Girard,[†,‡] Sandrine Perruchas,*,[†] Céline Gesset,[‡] Marc Chaigneau,[§] Laetitia Vieille,[†] Jean-Charles Arnault,[‡] Philippe Bergonzo,[‡] Jean-Pierre Boilot,[†] and Thierry Gacoin*,[†]

Laboratoire de Physique de la Matière Condensée (PMC), CNRS - Ecole Polytechnique, F-91128 Palaiseau cedex, France, CEA, LIST, Diamond Sensors Laboratory, F-91191 Gif-sur-Yvette, France, and Laboratoire de Physique des Interfaces et des Couches Minces (LPICM), CNRS - Ecole Polytechnique, F-91128 Palaiseau cedex, France

ABSTRACT Nanodiamond (ND) seeding is a well-established route toward the CVD (chemical vapor deposition) synthesis of diamond ultrathin films. This method is based on the deposition onto a substrate of diamond nanoparticles which act as pre-existing sp^3 seeds. Here, we report on a straightforward method to disperse diamond nanoparticles on a substrate by taking advantage of the electrostatic interactions between the nanodiamonds and the substrate surface coated with a cationic polymer. This layer-by-layer deposition technique leads to reproducible and homogeneous large-scale nanoparticle deposits independent of the substrate's nature and shape. No specific functionalization of the nanoparticles is required, and low concentrated solutions can be used. The density of NDs on the substrate can be controlled, as shown by in situ ATR-FTIR (attenuated total reflection Fourier transform infrared) analysis and QCM (quartz crystal microbalance) measurements. Highly dense and compact ND deposits can be obtained, allowing CVD growth of nanocrystalline diamond ultrathin films (70 nm) on various substrates. The synthesis of 3D structured and patterned diamond thin films has also been demonstrated with this method.

KEYWORDS: diamond nanoparticle • electrostatic grafting • nanocrystal seeding • CVD growth • diamond film

1. INTRODUCTION

Diamond is an attractive material, due to the combination of its outstanding mechanical, electrical, thermal, and optical properties. For scientific and technological applications, its high chemical and mechanical resilience, high surface stability, high thermal conductivity, and wide bandgap make diamond a promising candidate in the fields of electrochemistry, heat spreaders, biological platform, sensor devices, protective coatings, and so forth (1, 2). Several of these applications require very thin diamond layers (<100 nm) with a low surface roughness, for bioinert layers in biocell interfacing (3), for example, as well as for high-reactivity electrochemical applications (4) or electronics (5), thus increasing interest in an improved control of diamond nanocrystalline film growth.

Diamond deposition on non-diamond substrates is performed via two major processing steps. The first one, (i) nucleation, corresponds to the formation of diamond nuclei, i.e. the smallest thermodynamically stable islands, at the substrate surface. Nucleation procedures have been developed by performing either ex situ treatments on the substrate such as scratching or in situ methods before CVD (chemical vapor deposition) growth such as the BEN (bias enhanced nucleation) technique (6). While the first technique leads to an inhomogeneous density of the nuclei, the second one is limited by the conductivity of the substrate. Then the second step (ii) concerns the growth of the prepared nuclei, from a Volmer−Weber 3D growth mode (7). The best-quality layers are obtained using the MPCVD (microwave plasma chemical vapor deposition) technique in a H_2/CH_4 gas mixture. After coalescence of the growing crystals, a continuous film is obtained. Therefore, to achieve ultrathin films, very high densities of diamond seed crystals are needed on the substrate at the early stages of the CVD growth; studies have shown that values above 10^{11} objects $\cdot$ cm^{-2} are required (8). With respect to the nucleation step, one recently developed technique, so-called nanoseeding, involves the deposition of diamond nanoparticles on the substrate surface prior to growth, acting as pre-existing sp^3 seeds (8−10). In this case, the challenge is to get the highest density of nanodiamonds (NDs) on the surface with the highest homogeneity. The ideal case is obviously to reach the structure of a compact monolayer of diamond nanoparticles uniformly dispersed on the substrate.

Actually, increasing interest has been recently devoted to diamond nanoparticles, due to their multiple potential applications (11, 12). This research field has been recently

boosted by the development of large-scale productions which render this material widely available. There are two main methods to produce NDs: the first one is the detonation approach, where carbon-containing explosive charges are used in closed containers, leading to residues containing diamond (11, 13−15), and the second one is the mechanical grinding of synthetic HPHT (high pressure high temperature) micrometric diamond powders (16, 17). The latter is in fact the main source of commercially available diamond nanoparticles, mainly devoted to the huge market of polishing applications. With this method, single-crystal nanoparticles of 50 nm down to 4 nm can be obtained (18), whereas the primary size of detonation NDs is scaled at 5 nm. Another difference is that HPHT nanoparticles are not encapsulated in a pseudo-graphitic shell and are less sensitive to aggregation phenomena in comparison with detonation NDs. Note that doped nanoparticles, for instance with boron or nitrogen, are also accessible via the grinding production. Beyond their method of production, NDs are also characterized by their superficial chemistry, which mostly comes from the purification treatments performed after their synthesis (15). According to these treatments (chemical and/or thermal), different organic groups (ethers, hydroxyls, carboxylic acids, ...) are present at the particle surface (19). These oxygenated terminations confer the nanoparticles an electrostatic charge, which allows their spontaneous dispersion in aqueous solutions.

Different methods to disperse NDs onto a substrate have been reported in the literature, and most of the published works concern detonation nanodiamonds. Williams et al. have, for example, presented a method based on an ultrasonic seeding approach using ND powders in colloidal suspensions (20). Fox et al. have developed a technique based on inkjet technology to apply a solution of diamond nanoparticles on a silicon substrate (21). Spin coating of nanoparticle solutions, with or without polymers or surfactants or on mixing with sol−gel TiO_2, is also mentioned in several studies (22−24). For all these methods, the ND deposits are strongly dependent on various parameters such as the dispersion and concentration of the nanoparticles in the colloid solutions. Moreover, the spin-coating deposits may be strongly disturbed by the roughness of the substrate and fragile substrate may suffer from the ultrasonic treatment. One example of a controlled deposit has been reported in the literature and is based on the covalent bonding of NDs to the substrate. However, in this case, several chemical steps are required, such as fluorination of nanoparticles and silanization of the substrate (25).

Here we present a straightforward approach to disperse NDs on a substrate by taking advantage of the oxygenated terminations present at the diamond nanoparticle surface. As previously mentioned, these chemical groups provide the particle an electrostatic charge. Our approach relies on the use of an oppositely charged substrate: the nanoparticles can hence be simply deposited by electrostatic interactions. This technique, called layer-by-layer deposition, is known to prepare assemblies of nanoparticles (26, 27). With this

method, we have deposited negatively charged HPHT diamond nanoparticles on various substrates previously coated with a cationic organic polymer. By simple dipping of the coated substrate into the ND solution, electrostatic interactions ensure a spontaneous grafting of the particles onto the surface. A related method and its application to diamond nanoparticles have been already reported (28). Actually, ionic interactions are also reported to be involved in the strong adsorption of proteins on NDs (29, 30). On the basis of the same approach, a recent study has reported the assembly of ND clusters into films for biological applications (31).With our technique, reproducible and homogeneous nanoparticle films have been thus obtained in large scale on several kinds of materials and also on 3D structured substrates. The current approach also enables the fine control of the nanoparticle density on the substrate surface, up to the upper limit of a compact layer of NDs. The diamond nanoparticle deposition has been monitored using in situ ATR-FTIR (attenuated total reflection Fourier transform infrared) analysis, and quantitative estimation of the surface grafting has been realized using a QCM (quartz crystal microbalance). The nanoparticle deposits have been used as seeds for the CVD growth of diamond thin film. Surface patterning is also possible with this approach. It enables deposition of the nanoparticles on selected areas of the substrate and thus the growth of patterned nanocrystalline diamond thin films. The characterization of the diamond layers before and during the initial steps of the CVD growth has been realized by XPS (X-ray photoelectron spectroscopy), and analysis of a continuous diamond film was realized by Raman spectroscopy.

2. EXPERIMENTAL SECTION

2.1. Characterizations. 2.1.1. *SEM (Scanning Electron Microscopy) Analysis.* Electron microscopy experiments were performed using a FEG-SEM Hitachi 4800 operating between 1 and 10 kV. Diamond nanoparticle densities were determined by image analysis on SEM pictures using ImageJ software. The binary picture (black/white) is obtained by applying a threshold function on the gray level. The objects in binary are then counted by scanning the image until it finds the edge of an object. For isolated particles, the number of objects corresponds to the number of diamond nanoparticles. The diamond nanoparticle density is obtained by dividing the number of particles by the defined area (23).

2.1.2. *DLS (Dynamic Light Scattering) and ZP (Zeta Potential) Measurements.* The average size diameters (Z_{av}) evaluated by DLS and the zeta potential (ZP) values of the diamond nanoparticles in solution were recorded on a Malvern Zetasizer.

2.1.3. *QCM (Quartz Crystal Microbalance).* Measurements were performed on a Seiko EG&G QCA 922 instrument. The measurements were carried out at room temperature with AT cut crystal 9 MHz gold electrodes. First of all, two bilayers of PDDAC/PSS were deposited on the crystal for the charge enhancement of the crystal surface. Then, the electrode was vertically immersed in the aqueous polymer solution or in the diamond nanoparticle solution for 10 and 15 min, respectively. Before frequency measurement, the electrode was rinsed with ultrapure water and dried under nitrogen flux. In order to avoid saturation of the signal, the immersion time of the QCM electrode in the ND solution has been limited to 15 min. The

ACS APPLIED MATERIALS &INTERFACES

mass of particles, or polymer, adsorbed at the surface of the crystal is determined from the Sauerbrey equation (32):

$$\Delta F = \frac{-2f_0{}^2 \Delta m}{A\sqrt{\rho_q \mu_q}}$$

f_0 is the fundamental frequency of the crystal (9 MHz), ΔF is the frequency shift, and Δm is the mass adsorbed. $\mu_q = 2.947 \times 10^{11}$ g cm^{-1} s^{-2} and $\rho_q = 2.65$ g cm^{-3} are the shear modulus and the quartz density, respectively. $A = 0.392$ cm^2 is the active oscillation region of the crystal which is limited to the overlapping area of the front and rear Au electrodes.

2.1.4. ATR-FTIR (Attenuated Total Reflection Fourier Transform Infrared). Spectra were recorded using a Bomem MB 100 FTIR spectrometer equipped with a liquid-nitrogen-cooled MCT photovoltaic detector. Spectra are recorded with p polarization over the 1000−4000 cm^{-1} spectral range (4 cm^{-1} resolution). A Si sample with 45° bevels on the two opposite sides was used. This prism was prepared from double-side-polished float zone 800 Ω cm n-type (111) silicon (Siltronix).

2.1.5. XPS (X-ray Photoelectron Spectroscopy). Surface analysis was performed using an Omicron XPS spectrometer equipped with an Al Kα monochromated anode ($h\nu = 1486.6$ eV). The binding energy scale was calibrated versus the Au 4f 7/2 peak located at 84.0 eV (33). Samples were tilted (15°) to enhance the sensitivity to the surface. The penetration depths are given by the inelastic mean free paths for Si 2p and C 1s core levels, 3.2 and 3 nm, respectively (34). In addition to Si 2p and C 1s core levels, XEELS (X-ray energy loss spectroscopy) spectra were recorded at the carbon core level to give additional information about the carbon binding state.

2.1.6. Raman. The diamond film was analyzed using a high-resolution confocal Raman microscope (Labram HR800 from HORIBA Jobin Yvon) in the normal incident backscattering configuration, using the 100× objective. Excitation was provided by a tunable Ar laser from Melles Griot; 514 nm light was used for the sample characterization. In order to avoid sample heating, the incident laser power was less than 1 mW, collection time 1 s, with 10 accumulations.

2.2. Synthesis. 2.2.1. Diamond Nanoparticles. HPHT (high pressure high temperature) diamond nanoparticles were purchased from Van Moppes (Syndia SYP 0-0.05 and SYP 0-0.02 GAF). Different nanoparticle solutions were used and are described below with corresponding DLS size distribution histograms reported Figure S2 in the Supporting Information.

2.2.1.1. ND-50. SYP 0-0.05 powder was dispersed in ultrapure water and sonicated for 10 min: $c = 1$ g L^{-1}, $Z_{av} = 50$ nm, and ZP = −44 mV.

2.2.1.2. ND-30. SYP 0-0.02 GAF aqueous solution was used as received: $c = 3$ g L^{-1}, $Z_{av} = 30$ nm, and ZP = −48 mV.

2.2.1.3. ND-15. This species was obtained from size selection of ND-50 solution achieved by centrifugation (11 000 rpm for 180 min): $c = 0.4$ g L^{-1}, $Z_{av} = 15$ nm, and ZP = −36 mV.

2.2.2. ND Films. Poly(diallyldimethylammonium chloride) (PDDAC, molecular weight 100 000−200 000) was purchased from Aldrich and used as received. Silicon substrates were treated with piranha solution H_2SO_4/H_2O_2 30 % (3/1 v/v) for 20 min. After intense washing with water, the substrate was introduced in the PDDAC polymer aqueous solution (diluted in water 1/10 v/v) for 10 min. The substrates were washed with water again and then immersed in the ND solution (various times). Finally, the substrates were washed vigorously by flushing water for several minutes and dried under an N_2 flux. Substrates were vertically suspended in the polymer or ND solutions. Surface patterning of the polymer was achieved by pure Argon RF plasma (42 sccm Ar, 50 W, 5 s), through a metallic mask.
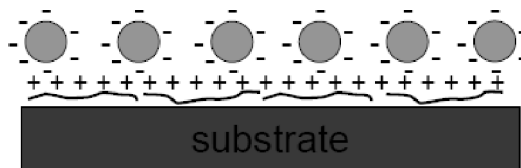

FIGURE 1. Principle of the electrostatic grafting of negatively charged diamond nanoparticles on cationic polymer-coated substrate.

2.3. CVD (Chemical Vapor Deposition) Growth Conditions. Parameters were tuned with a pressure of 40 mbar, at a CH_4/H_2 ratio of 1/99. The microwave power was adjusted to 1.1 kW in order to reach a temperature of 750 °C measured in situ using an optical pyrometer (Ircon Modline 3 series 3L). For growth on quartz and gold substrates (Figure 10), the pressure and microwave power were reduced to 20 mbar and 600 W, respectively, in order to limit the temperature to 500 °C.

3. RESULTS AND DISCUSSION

3.1. Synthesis and Characterization of the Diamond Nanoparticle Layers. When dispersed in water, HPHT nanoparticles have a zeta potential value around −40 mV whatever their size (see the Experimental Section). This negative charge is attributed to carboxylic acid groups present at the diamond surface (35). FTIR analysis (see below) confirms this result, with a broad band centered at 1775 cm^{-1} (C=O stretching bond) attesting to the presence of carboxylic acid groups and acid anhydride functionalities (36). Therefore, in order to disperse these HPHT nanoparticles on a substrate by means of attractive electrostatic interactions, the substrate requires an opposite electrostatic charge. To confer positive electrostatic charge to the substrate, the cationic polymer PDDAC (poly(diallyldimethylammonium chloride)) has been chosen to coat the substrate surface. This polymer is commonly used in layer-by-layer film processing (26). First, the substrate is cleaned with a piranha treatment followed by intense rinsing with water. The substrate is then immersed in the aqueous polymer solution, rinsed with water, and then immersed in the diamond nanoparticle solution, rinsed again with water, and finally dried under nitrogen flux. A schematic representation of the electrostatic grafting of the diamond nanoparticles onto the polymer-coated substrate is given in Figure 1.

The ND films obtained on silicon substrates were analyzed by SEM (scanning electron microscopy) and are shown in Figure 2. A homogenous and reproducible layer of diamond nanoparticles is obtained on the polymer-coated surface (Figure 2a) after an immersion time of 15 min in the ND-50 solution (see the Experimental Section). This dense coating of nanoparticles is homogeneous on a 10×10 mm substrate. Individual nanoparticles are clearly observed on the surface with no aggregate. For comparison, Figure 2b shows a silicon substrate treated with a piranha solution but without the polymer coating, after immersion in the same diamond nanoparticle solution during the same time. As clearly illustrated by this picture, the spontaneous deposition of nanoparticles at the surface is very weak, inhomogeneous, and not reproducible. These results demonstrate the efficiency of the polymer coating for the nanoparticle grafting, which is driven by electrostatic interactions. These interac-
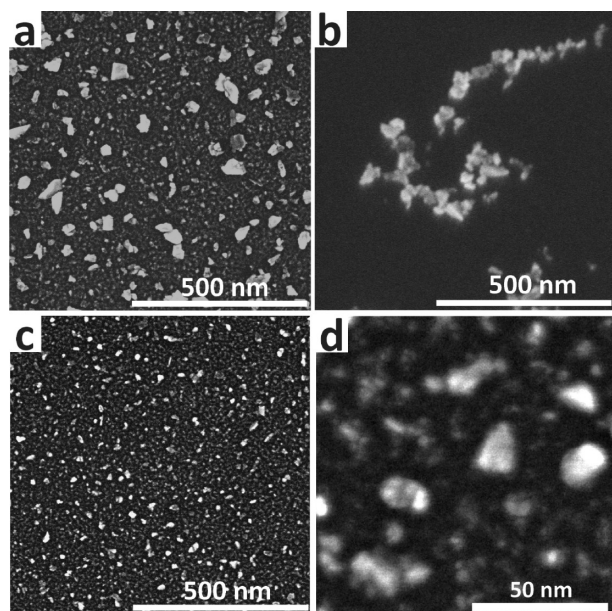
FIGURE 2. SEM pictures of a silicon substrate after 15 min of immersion in ND-50 solution: (a) with PDDAC polymer coating; (b) without PDDAC coating; (c, d) a silicon substrate coated with PDDAC after 15 min of immersion in ND-15 solution.

tions are stronger compared to inter-ND interactions leading to the deposition of nanoparticles without aggregation. However, as shown in Figure 2a, a wide dispersion in size of the NDs is observed on the surface, including nanoparticles with sizes close to 50 nm. This is in accordance with the DLS measurements done on the ND-50 aqueous solution exhibiting a particle size distribution from 50 nm down to 4 nm (Figure S2, Supporting Information). The use of ND with narrower size distribution and smaller size presents two major advantages for diamond CVD growth: higher densities of sp^3 seeds can be reached, and thinner diamond films with lower roughness may be obtained, as coalescence will be reached faster. It is worth mentioning that the growth of ultrathin nanocrystalline diamond films (<130 nm) at low temperature have been reported and was attributed to the use of substrates with high seeding density obtained by the ultrasonic process (37). In order to remove the largest particles from the solution, a size selection has been performed using centrifugations (see the Experimental Section). From 50 nm, the average size of the particles in the solution has been reduced to 15 nm (ND-15). Figure 2c presents the coating obtained with this ND-15 solution. The surface is covered by smaller particles (≤15 nm) in a dense framework. From Figure 2d, an estimation of the particle density can be calculated, with a value up to 3×10^{11} ND · cm^{-2}. This value competes with the highest densities reported in the literature for detonation NDs deposited on a silicon wafer by ultrasonic treatment (1, 20).

By varying the concentration of the nanoparticles in solution and/or the time of immersion, it is also possible to control the ND density on the surface. As illustrated on Figure 3a,b, lowering the time of immersion from 1 min to 5 s, for the same ND solution concentration, leads to lower nanoparticle surface coverage. The ND density decreases from 1×10^{11} to 3×10^{10} ND · cm^{-2}. In the same way, as

shown in Figure 3c with respect to Figure 3b, an immersion in a solution at a diluted concentration (1/10) for the same duration (5 s) leads to a lower density of 2×10^9 ND · cm^{-2}. Therefore, this method of deposition allows an accurate control of the ND density deposited on a surface. Furthermore, since ND density can be increased by adjusting the time of immersion, this method can be particularly attractive for obtaining dense layers from very dilute solutions of nanoparticles (for example, after ultracentrifugation (18)). This method, which ensures a good adhesion of ND onto a silicon substrate (in terms of stability to water rinsing, see the Experimental Section and ATR-FTIR measurements), has also been performed on other types of substrates, including gold, platinum, chromium (Figure 3), and quartz, giving rise to similar layers in terms of homogeneity and reproducibility. This latter point is of very great interest, considering that this seeding method is not limited to conductive materials, as opposed to e.g. the bias enhanced nucleation technique.

In order to monitor the ND grafting to the PDDAC polymer-coated substrate, in situ ATR-FTIR measurements have been performed. The analysis has been carried out using a hermetic cell composed of a silicon wafer onto which the solutions can circulate. The IR signal is thus detected after multiple reflections in the substrate whose surface is modified by the grafting of species present in the solution. The deposition of the diamond nanoparticles has been thus monitored step by step, and the corresponding spectra are reported in Figure 4. First, water has been circulated in the cell and the reference spectrum has been recorded (Supporting Information). For all spectra shown, this reference has been subtracted in order to enhance the signals of both polymer and NDs which can be hindered by an intense water signal. The water solution was then replaced by the PDDAC polymer solution. As shown by curve 1 in Figure 4a, a very low signal has been detected so that the polymer concentration was increased (×10) and a peak at 1472 cm^{-1} (curve 2, Figure 4a) was easily detected corresponding to the CH_3 and CH_2 groups of the polymer (FTIR spectra of the polymer in KBr pellets in the Supporting Information). After rinsing with water (curve 3, Figure 4a), the intensity of the peak decreases, suggesting that only a small amount of polymer remains grafted to the silicon surface. The ND solution was then introduced and a peak at 1788 cm^{-1} was observed (curve 4, Figure 4a) corresponding to the C=O vibration of carbonyl groups on the diamond surface (FTIR spectra of ND in KBr pellets in the Supporting Information). As shown in Figure 4b, by recording spectra every 5 min, the intensity of this peak increases regularly until about 25 min, after which its intensity remains almost constant. The penetration depth of the signal is about 380 nm under these experimental conditions (38) and is larger than the interface probed (PDDAC/ND-15); thus, the saturation observed is not linked to signal saturation. Therefore, the maximum intensity reached for the ATR signal after 25 min suggests a full coverage of the surface by NDs. After deep rinsing with water, the peak intensity does not change, thus implying that
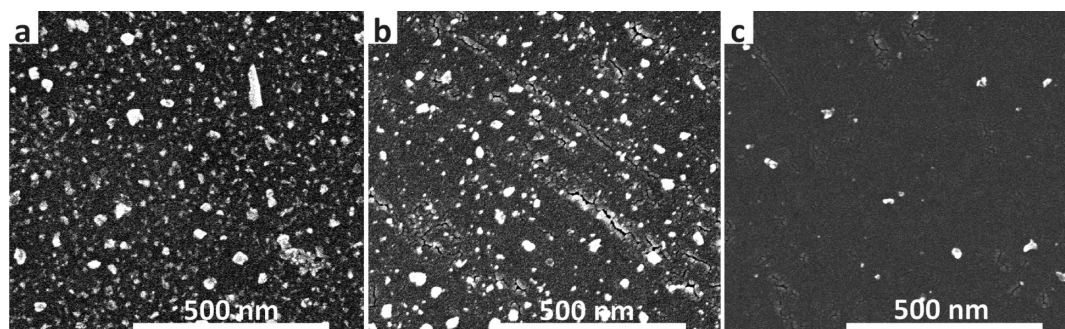
FIGURE 3. SEM pictures of diamond nanoparticles deposited on a PDDAC-coated Cr substrate using (a) ND-30 solution over 1 min, (b) ND-30 solution over 5 s, and (c) ND-30 solution diluted c/10 over 5 s.
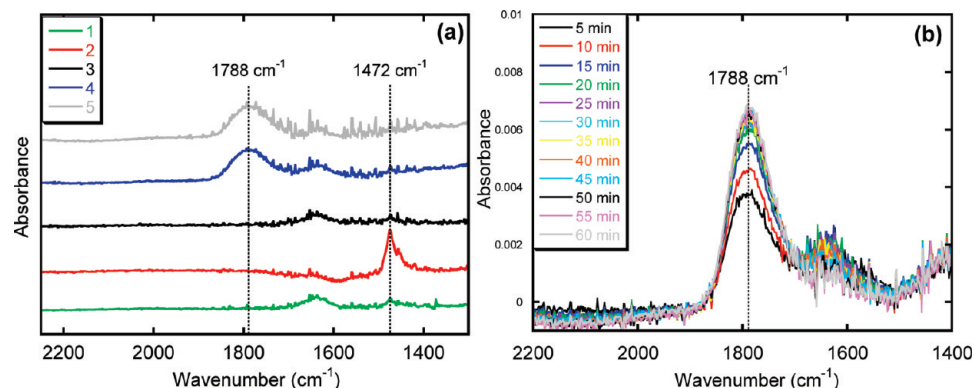

FIGURE 4. ATR-FTIR spectra of PDDAC polymer and diamond nanoparticle (ND-15) depositions on Si substrate. (a) Successive steps for the ND film synthesis by circulating solutions in the cell: curve 1, polymer solution (10 min); curve 2, concentrated polymer solution (10 min); curve 3, water (10 min); curve 4, ND-15 solution (60 min); curve 5, water (10 min). (b) Diamond nanoparticle signal recorded in real time when the ND solution is circulating (5−60 min).
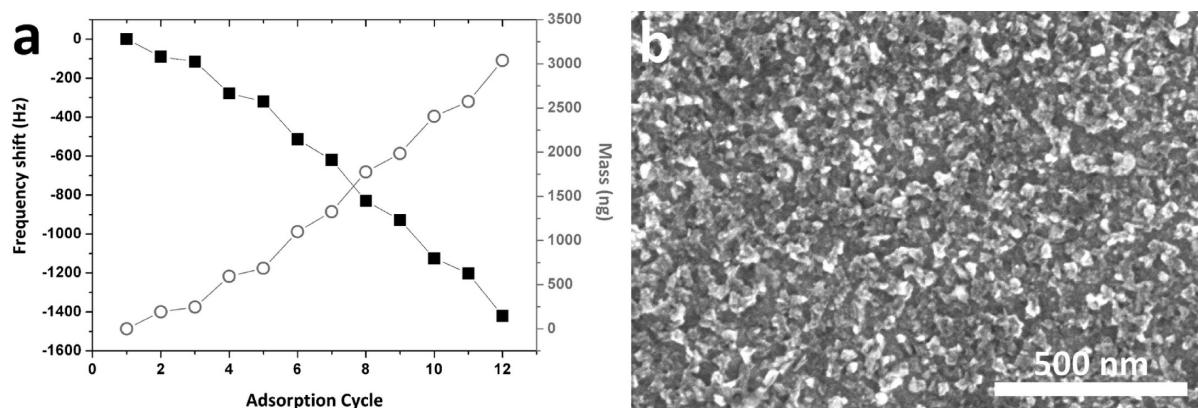

FIGURE 5. (a) QCM measurements, giving the frequency shift and calculated mass adsorbed according to each deposited layer of ND-30 and PDDAC polymer. The first adsorption corresponds to deposition of PDDAC. (b) SEM picture of six ND-30/PDDAC layers.

NDs are effectively grafted on the surface (curve 5, Figure 4a). This study shows that very low amounts of polymer remain necessary to graft the NDs to the substrate surface. In this experiment, using a specific concentrated solution of ND (ND-15), the saturation of the surface by the nanoparticles is almost reached after 25 min. As already mentioned, this study shows that the ND surface density can be controlled by adjusting the immersion time of the substrate in the solution. The efficient electrostatic interactions between the nanoparticles and the PDDAC polymer is evidenced by the stability of the ND signal upon washing with water.

Quartz crystal microbalance (QCM) measurements were performed in order to estimate, in a quantitative way, the deposition of diamond nanoparticles onto the substrate. This technique allows an accurate measurement, since it is capable of detecting mass changes in the $ng \cdot cm^{-2}$ range. Nevertheless, to improve the precision of the result, QCM measurements have been performed on successive depositions. Several adsorptions were therefore monitored by repeating the deposition sequences of polymer/NDs. Figure 5a reports the evolution of the frequency shift and the corresponding calculated mass of diamond particles or polymer for each deposition on the quartz. The substrate was first coated with the polymer so that the second layer deposited corresponds to NDs. Whatever the nature of the coating, i.e. diamond or polymer, a regular increase of the mass is observed at each adsorption, thus demonstrating
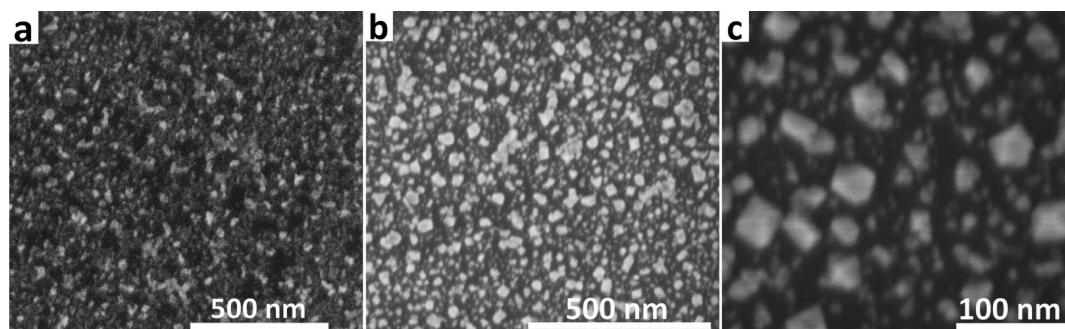
FIGURE 6. SEM pictures of ND-15 deposited on PDDAC coated Si substrate (a) before and (b, c) after 10 min of CVD plasma growth.

the high sensitivity of the method. The average calculated masses for one polymer and one diamond nanoparticle layer are 138 and 364 ng, respectively (see the Experimental Section). On the basis of its density ($\rho_{PDDAC} = 1.2 \text{ g} \cdot \text{cm}^{-3}$), the calculated layer thickness of each polymer film attains 3.2 nm. This value points out the thinness of the layer coated onto the substrate required to graft the diamond nanoparticles and agrees with the low signal detected by FTIR analysis. Concerning the calculated mass of NDs deposited at each cycle, a short calculation taking into account the average diameter of the particles studied (ND-30) leads to a value of $3 \times 10^{10} \text{ ND} \cdot \text{cm}^{-2}$ deposited on the substrate at each cycle. Figure 5b shows the SEM picture of the layer obtained on the electrode after 12 adsorptions, i.e. 6 polymer/ND layers. The surface is entirely covered by a thick layer of nanoparticles and appears rough. A slight increase of the mass deposited is observed after each layer (Figure 5a). This phenomenon is probably due to the expansion of the accessible surface area, which is correlated to the increasing roughness generated by the accumulation of particles at the surface. In addition to provide quantitative measurement of the ND deposits, this study demonstrates the feasibility of fabricating thick ND films based on multilayer depositions of diamond nanoparticles on a substrate. These assemblies could lead to diamond materials with high surface area.

3.2. CVD Growth of Nanocrystalline Diamond Thin Films.
Highly dense and homogenous ND layers obtained by our method are ideal substrates for CVD growth of diamond thin film. Indeed, higher seed densities on the substrate lead to faster coalescence between the crystallites and thus to the ability to synthesize thinner nanocrystalline diamond layers. First, a short CVD growth (10 min, with parameters given in the Experimental Section) was performed on a ND film deposited on a silicon substrate (ND-15 solution). The duration of the growth has been limited in order to avoid a too early coalescence of the crystals and be able to clearly observe the growth of the nanoparticles. Figure 6 shows the SEM images of this sample before (a) and after the short CVD plasma (b, c). In Figure 6b,c, an enlargement of the nanoparticles clearly occurs, associated with faceting of the crystallites (Figure 6c). The development of diamond nanocrystal faceting indicates diamond growth on the particles, which is commonly observed at the early stages of the CVD process (37). When longer CVD growths are performed (45 min using the same experimental conditions), a continuous diamond film with well-faceted grains
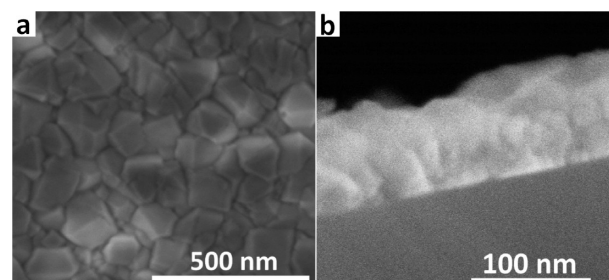

FIGURE 7. SEM images giving (a) a top view of the diamond thin film (ND-30/PDDAC) after 45 min of CVD plasma growth and (b) a cross-section view of two ND-30/PDDAC layers after 25 min of CVD plasma growth.

can be obtained, as shown in Figure 7a. From optical analyses using laser reflectometry (39), a thickness of 140 nm has been measured for this film. The coalescence of the crystallites under these experimental conditions confirms the high density of nanoparticles on the surface acting as seeds during the CVD growth.

As previously mentioned, this seeding method also allows the formation of multilayers of NDs on a surface by repeating the deposition process. As the ND solutions used are composed of nanoparticles with different sizes, multilayer depositions could increase the diamond seeds. Indeed, a short CVD plasma growth step (25 min, with parameters given in the Experimental Section) realized on a substrate with two successive ND/polymer layers leads to a continuous thin diamond layer shown in cross section in Figure 7b. In this film of 70 nm thickness, individual ND particles can be distinguished at the Si/diamond interface.

Another advantage of using the polymer for the ND deposition concerns the possibility to pattern the surface. Different techniques are reported in the literature for diamond surface patterning, including selective deposition, ablation, dry etching, and replication (40). A lithographic technique has been also recently reported to obtain patterned diamond growth (41). Here, the method simply consists of performing an Ar plasma etching of the polymer layer through a mask, leaving coated and uncoated areas on the substrate. Thus, after immersion of the substrate in the ND solution, the nanoparticles are selectively grafted on the polymer-coated areas. Figure 8a shows a selective deposition of diamond nanoparticles on a silicon substrate, by means of polymer patterning using a metallic grid. The picture has been taken in a wet atmosphere in order to condense water drops on the substrate; diamond nanoparticles and bare
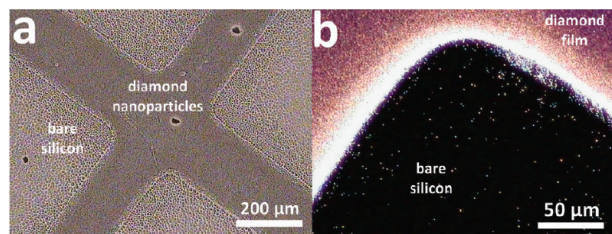
FIGURE 8. Optical microscopy photos of a ND-15/PDDAC patterned surface on Si (a) observed in a wet atmosphere before CVD plasma growth and (b) after 25 min of CVD plasma growth.

silicon areas can thus be distinguished by their different wettability properties. After CVD growth (25 min, with parameters given in the Experimental Section), the patterning is preserved with the diamond film grown only on the areas where NDs were grafted being the replica of the mask used (Figure 8b). High diamond growth selectivity is thus achieved, since only a few residual diamond nanoparticles can be observed on the etched areas. Using this method, the pattern is only limited by the dimension of the mask used during the Ar plasma etching. Furthermore, as compared to lithographic and etching methods for post-growth patterning, the technique presented here is easily achievable and does not require any tedious chemical etching step of the diamond, often very chemically resilient.

XPS analysis was performed on the diamond films in order to probe if the polymer may affect the quality of the grown diamond. In fact, the presence on the substrate prior to growth of carbonic species provided by the polymer may somehow initiate the formation of impurities (sp^2, amorphous carbon), which may alter the diamond quality. Also, because of the high temperatures used for growth (750 °C typically), a diffusion of the carbon into the silicon substrate may lead to the formation of silicon carbide (42, 43). Figure 9 presents C 1s and Si 2p spectra of a diamond nanoparticle film on silicon substrate, before and after a short CVD growth step (10 min, with parameters given in the Experimental Section). Before growth, the C 1s spectrum of the nanoparticles exhibits two main components at about 285 and 286 eV, attributed to a C−C sp^3 bond and oxygenated terminations, respectively (Figure 9a). An exaltation of the "C−O" bonds is observed on nanoparticles, which can be related to the geometry of the objects: since the probed depth (a few nanometers) remains very small as compared with the mean diameter of the particles (Z_{av} = 50 nm), the surface bonds do appear exalted. The plasma induces a strong modification of the C 1s spectra; the main peak is at 286 eV before growth, whereas it is at 284.8 eV after growth. This later value is in accordance with those measured on diamond thin films, exhibiting the presence of C−C sp^3 bonds at the surface (42). At higher binding energies, the C 1s spectrum also reveals the presence of oxygen groups at the surface, as small contributions are visible around 286 and 287 eV (42). The presence of oxygen species on the surface may be attributed to the exposure of the sample to air between the short CVD growth and the XPS analysis. In order to confirm diamond growth onto the particles, a XEELS spectrum has been recorded at the C 1s core level and is

shown in Figure 9c. The presence of C−C sp^3 bonds is confirmed with the clear signature of surface and bulk diamond plasmons at 24.5 and 33.5 eV, respectively (44). Si 2p spectra have been recorded to probe the effect of the polymer on the substrate during the CVD plasma and are shown in Figure 9b. In addition to the Si−Si peak (99.2 eV), a well-defined contribution of silicon oxides (103.5 eV) is exhibited for both spectra. The exaltation of SiOx after the short CVD growth can be related to a modified reactivity of the bare Si to the atmosphere before and after the CVD plasma (SEM picture of Figure 6c). The lack of silicon carbide, usually observed around 100.8 eV, is evidenced. Furthermore, no contribution of C−Si is observed on the C 1s spectra, usually found between 283 and 282 eV. In summary, the analyses of silicon and carbon XPS core level spectra and XEELS all confirm that the polymer does not affect the growth of diamond. No residues of polymer seem to be produced under plasma conditions. In addition, despite the presence of carbonic species on the substrate and the elevated temperatures reached (above 750 °C), the interface between the diamond layer and the silicon is free from silicon carbide. From QCM experiments, which have shown that the polymer layer thickness remains close to 3 nm, it may be suggested that the polymer is immediately removed from the surface by the plasma at the beginning of the growth. Note that it is also possible to remove the polymer by Ar plasma etching before the growth. Actually, previous studies have shown that polymer present at the substrate surface can act as a carbon source, enhancing the diamond nucleation and accelerating homogenous CVD growth (45). Due to the small amount of polymer present in our case (monolayer), this phenomenon may take place but with less influence on the diamond structure.

Raman analysis was performed on a diamond film grown on silicon substrate (60 min, with parameters given in the Experimental Section). The spectrum shown in Figure 10 presents a major peak at 1332 cm^{-1} corresponding to the diamond phase. The two other less resolved peaks at around 1135 and 1450 cm^{-1} are assigned to *trans*-polyacetylene segments at grain boundaries and surfaces, characteristic of nanocrystalline diamond films (46).

Finally, seeding on a 3D structured substrate has also been performed with our method. Note the ultrasonic techniques has been recently used to grow structured diamond films (47). In our case, three ND/PDDAC layers have been deposited on a quartz substrate with gold patterns of 100 nm thickness. Parts a and b of Figure 11 show the growth of the crystallites after a CVD growth (45 min, with conditions given in the Experimental Section). A homogeneous layer is obtained on both the quartz and gold areas. This technique of seeding is thus independent of the substrate chemical nature. Figure 11b also reveals that particles have covered the top and the edges of the gold pattern. This result is very promising, and more complex 3D diamond structures can be considered with this technique.
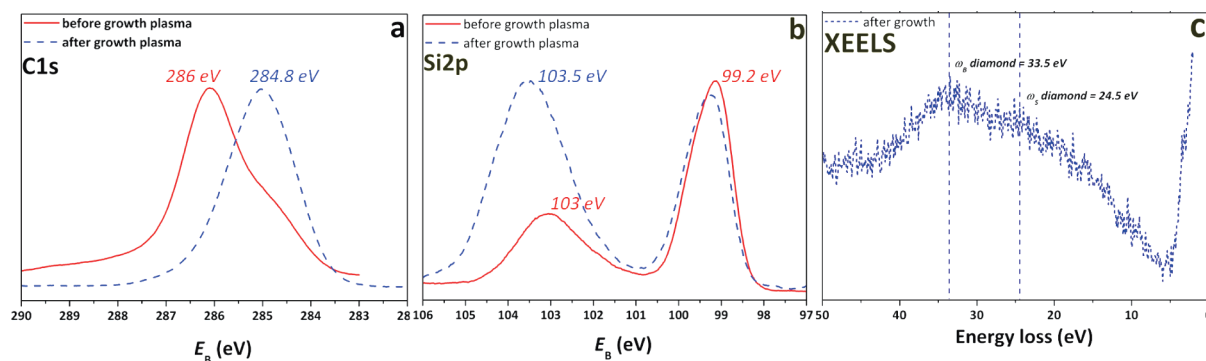
FIGURE 9. XPS analysis giving (a) C 1s and (b) Si 2p core level spectra (normalized) and (c) XEELS spectra (C—C sp³ peak as the energy loss origin) of diamond nanoparticles (ND-50) deposited on PDDAC-coated Si substrate before (solid line) and after (dashed line) 10 min of CVD plasma growth (see the Experimental Section).
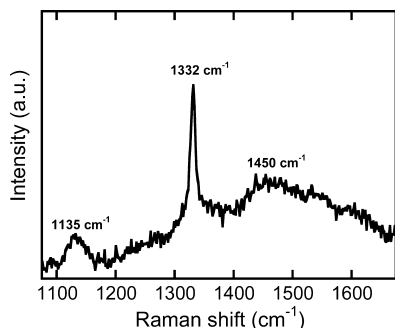

FIGURE 10. Raman spectra of the diamond film (ND-30/PDDAC) on a silicon substrate after 60 min of CVD plasma growth.
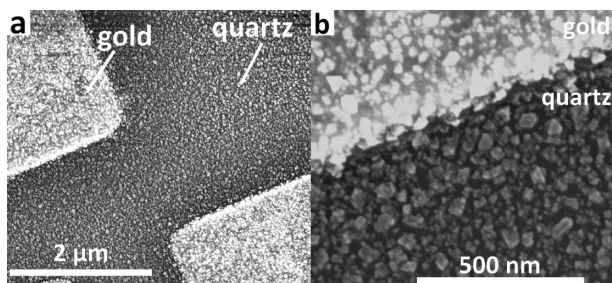

FIGURE 11. SEM pictures of three ND-30/PDDAC layers deposited on a quartz substrate with 100 nm thick gold patterns, after 45 min of CVD plasma growth.

4. CONCLUSION

We have reported here a straightforward approach to disperse diamond nanoparticles on a substrate by taking advantage of the electrostatic interactions between them and the substrate surface. In fact, NDs bear an electrostatic charge due to specific organic groups present at their surface that is used to drive them to a substrate coated with an ultrathin layer of oppositely charged organic polymer. Dense, reproducible, and homogeneous nanoparticle deposits have thus been obtained, confirmed in a quantitative and qualitative way by in situ ATR-FTIR analysis and QCM measurements.

This easy method presents several advantages. Homogeneous large-scale deposits can be obtained, as shown by SEM analysis. Various chemical natures of substrates can be used, and seeding on 3D structured substrates has been demonstrated. Moreover, no functionalization of the ND is required. The nanoparticle density on the surface can be also controlled by tuning the concentration of the ND solution and the time of immersion. When both parameters are increased, a compact monolayer of NDs can be reached. By this method, layers can be also obtained using solutions of low ND concentrations. Finally, by repetition of the deposition process, multilayers of diamond nanoparticles can be easily obtained, leading to higher diamond seed densities. Surface patterning is also possible with this technique, by selective deposition of the nanoparticles on the substrate.

NDs assisted CVD growth of diamond thin films has also been demonstrated with this method. Nanocrystalline coalescent diamond thin films of very low thickness (70 nm) have been obtained, and XPS analysis has confirmed that the polymer does not affect the growth. Raman analysis of a continuous diamond film revealed an important contribution for the sp³ phase. Thinner films could be synthesized with NDs of reduced sizes. With their 5 nm size, detonation NDs are also ideal objects for this sp³ seeding approach. Grafting of such NDs with our technique is currently in progress.

In summary, this technique constitutes a reliable and versatile seeding method, enabling structured ultrathin diamond layers to be grown, and this method can be scaled up to large-area substrates. Finally, these ND deposits could find applications in other fields. For instance, diamond nanoparticle thick films obtained by multilayer deposition could be useful for sensor applications where high-surface-area materials are required.

Supporting Information Available: Figures giving FTIR spectra in KBr pellets (ND-50 and PDDAC polymer), ATR-FTIR spectra of Si substrate in H_2O, and the DLS size distribution of ND solutions used. This material is available free of charge via the Internet at http://pubs.acs.org.

REFERENCES AND NOTES

(1)   Philip, J.; Hess, P.; Feygelson, T.; Butler, J. E.; Chattopadhyay, S.; Chen, K. H.; Chen, L. C. *J. Appl. Phys.* **2003**, *93*, 2164–2171.
(2)   Dong, C.; Chen, S.; Chiou, J.; Chen, Y.; Guo, J.; Cheng, H.; Lin, I.; Chang, C. *Diamond Relat. Mater.* **2008**, *17*, 1150–1153.
(3)   Grausova, L.; Bacakova, L.; Kromka, A.; Vanecek, M.; Rezek, B.; Lisa, V. *Diamond Relat. Mater.* **2009**, *18*, 258–263.

(4) Vanhove, E.; De Sanoit, J.; Arnault, J. C.; Saada, S.; Mer, C.; Mailley, P.; Bergonzo, P.; Nesladek, M. *Phys. Status Solidi A* **2007**, *204*, 2931–2939.

(5) Nebel, C. E.; Yang, N.; Uetsuka, H.; Yamada, T.; Watanabe, H. *J. Appl. Phys.* **2008**, *103*, 13712.

(6) Yugo, S.; Kanai, T.; Kimura, T. *Diamond Relat. Mater.* **1992**, *1*, 929–932.

(7) Liu, H.; Dandy, D. S. In *Diamond Chemical Vapour Deposition: Nucleation and Early Growth Stages*; Bunshah, R. F., McGuire, G. E., Rossnagel, S. M., Eds.; Noyes: Park Ridge, NJ, 1995; Chapter 7.

(8) Daenen, M.; Williams, O. A.; D'Haen, J.; Haenen, K.; Nesládek, M. *Phys. Status Solidi A* **2006**, *203*, 3005–3010.

(9) Vul', A. Ya.; Golubev, V. G.; Grudinkin, S. A.; Krueger, A.; Naramoto, H. *Tech. Phys. Lett* **2002**, *9*, 787–789.

(10) Yara, T.; Makita, H.; Hatta, A.; Ito, T.; Hiraki, A. *Jpn. J. Appl. Phys.* **1995**, *34*, L312–L315.

(11) Krueger, A. *Adv. Mater.* **2008**, *20*, 2445–2449.

(12) Baidakova, M.; Vul, A. *J. Phys. D: Appl. Phys.* **2007**, *40*, 6300–6311.

(13) Shenderova, O. A.; Zhirnov, V. V.; Brenner, D. W. *Crit. Rev. Solid State Mater. Sci.* **2002**, *27*, 227–356.

(14) Danilenko, V. V. *Phys. Solid State* **2004**, *46*, 595–599.

(15) Pichot, V.; Comet, M.; Fousson, E.; Baras, C.; Senger, A.; Le Normand, F.; Spitzer, D. *Diamond Relat. Mater.* **2008**, *17*, 13–22.

(16) Niwase, K.; Tanaka, T.; Kakimoto, Y.; Ishihara, K. N.; Shingu, P. H. *Mater. Trans.* **1995**, *36*, 282–288.

(17) Iijima, S. Japanese Patent JP 04132606, 1992.

(18) Morita, Y.; Takimoto, T.; Yamanaka, H.; Kumekawa, K.; Morino, S.; Aonuma, S.; Kimura, T.; Komatsu, N. *Small* **2008**, *4*, 2154–2157.

(19) Krueger, A.; Liang, Y.; Jarre, G.; Stegk, J. *J. Mater. Chem.* **2006**, *16*, 2322–2328.

(20) Williams, O. A.; Douhéret, O.; Daenen, M.; Haenen, K.; Osawa, E.; Takahashi, M. *Chem. Phys. Lett.* **2007**, *445*, 255–258.

(21) Fox, N. A.; Youh, M. J.; Wang, W. N.; Steeds, J. W.; Cheng, H.-F.; Lin, I.-N. *Diamond Relat. Mater.* **2000**, *9*, 1263–1269.

(22) Hanada, K.; Matsuzaki, K.; Sano, T. *Surf. Sci.* **2007**, *601*, 4502–4505.

(23) Scorsone, E.; Saada, S.; Arnault, J. C.; Bergonzo, P. *J. Appl. Phys.* **2009**, *106*, 014908.

(24) Daenen, M.; Zhang, L.; Erni, R.; Williams, O. A.; Hardy, A.; Van Bael, M. K.; Wagner, P.; Haenen, K.; Nesladek, M.; Tendeloo, G. V. *Adv. Mater.* **2009**, *21*, 670–673.

(25) Liu, Y.; Khabashesku, V.; Halas, N. *J. Am. Chem. Soc.* **2005**, *127*, 3712–3713.

(26) Mamedov, A.; Ostrander, J.; Aliev, F.; Kotov, N. A. *Langmuir* **2000**, *16*, 3941–3949, and references therein. .

(27) Xue, W.; Cui, T. *Nanotechnology* **2007**, *18*, 145709.

(28) (a) Gilbert, D. R.; Carasso, M. L.; Demkowicz, P. A.; Singh, R. K.; Adair, J. H. *J. Elec. Mater.* **1997**, *26* (11), 1326–1330. (b) Adair, J. H.; Singh, R. K.; Rajiv, K. US Patent 24529394A, 1995.

(29) Huang, L.-C. L.; Chang, H.-C. *Langmuir* **2004**, *20*, 5879–5884.

(30) Kong, X. L.; Huang, L. C. L.; Hsu, C.-M.; Chen, W.-H.; Han, C.-C.; Chang, H.-C. *Anal. Chem.* **2005**, *77*, 259–265.

(31) Huang, H.; Pierstorff, E.; Osawa, E.; Ho, D. *ACS Nano* **2008**, *2*, 203–212.

(32) Sauerbrey, G. *Z. Phys.* **1959**, *155*, 206–222.

(33) Seah, M. P. *Surf. Interface Anal.* **1989**, *14*, 488.

(34) Tanuma, S.; Powell, C. J.; Penn, D. R. *Surf. Interface Anal.* **1988**, *11*, 577–589.

(35) Xu, Y. Y.; Yu, Z. M.; Zhu, Y. M.; Wang, B. C. *Diamond Relat. Mater.* **2005**, *14*, 206–212.

(36) Chung, P.-H.; Perevedentseva, E.; Tu, J.-S.; Chang, C.; Cheng, C.-L. *Diamond Relat. Mater.* **2006**, *15*, 622–625.

(37) (a) Kromka, A.; Potocky, S.; Cermak, J.; Rezek, B.; Potmesil, J.; Zemek, J.; Vanecek, M. *Diam. Relat. Mater.* **2008**, *17*, 1252–1255. (b) Kromka, A.; Rezek, B.; Remes, Z.; Michalka, M.; Ledinsky, M.; Zemek, J.; Potmesil, J.; Vanecek, M. *Chem. Vap. Deposition* **2008**, *14*, 181–186.

(38) Vahur, S.; Knuutinen, U.; Leito, I. *Spectrochim. Acta, Part A* **2009**, *73*, 764–771.

(39) Saada, S.; Pochet, S.; Rocha, L.; Arnault, J. A.; Bergonzo, P. *Diamond Relat. Mater.* **2009**, *18*, 707–712.

(40) Ding, G.; Mao, H.; Cai, Y.; Zhang, Y.; Yao, X.; Zhao, X. *Diamond Relat. Mater.* **2005**, *14*, 1543–1548.

(41) Kromka, A.; Babchenko, O.; Rezek, B.; Ledinsky, M.; Hruska, K.; Potmesil, J.; Vanecek, M. *Thin Solid Films* **2009**, doi:10.1016/j.tsf.2009.06.014.

(42) Arnault, J. C.; Saada, S.; Nesladek, M.; Williams, O.; Haenen, K.; Bergonzo, P.; Osawa, E. *Diamond Relat. Mater.* **2008**, *17*, 1143–1149.

(43) Arnault, J. C.; Saada, S.; Delclos, S.; Rocha, L.; Intiso, L.; Polini, R.; Hoffman, A.; Michaelson, S.; Bergonzo, P. *Chem. Vapor Depos.* **2008**, *14*, 187–195.

(44) Wang, Y.; Hoffman, R. W.; Angus, J. C. *J. Vac. Sci. Technol. A* **1990**, *8*, 2226–2230.

(45) Kromka, A.; Babchenko, O.; Kozak, H.; Hruska, K.; Rezek, B.; Ledinsky, M.; Potmesil, J.; Michalka, M.; Vanecek, M. *Diamond Relat. Mater.* **2009**, *18*, 734–739.

(46) (a) Ferrari, A. C.; Robertson, J. *Phys. Rev. B* **2001**, *63*, 1214051. (b) Kuzmany, H.; Pfeiffer, R.; Salk, N.; Gunther, B. *Carbon* **2004**, *42*, 911–917. (c) Ballutaud, D.; Kociniewski, T.; Vigneron, J.; Simon, N.; Girard, H. *Diamond Relat. Mater.* **2008**, *17*, 1127–1131.

(47) Kromka, A.; Rezek, B.; Kalbacova, M.; Baresova, V.; Zemek, J.; Konak, C.; Vanecek, M. *Adv. Eng. Mater.* **2009**, *11* (7), B71–B76.